Mathematical modelling of thermal interactions during freezing: Effects on product morphology and drying behaviour

(Article begins on next page)

08 July 2025

Mathematical modelling of thermal interactions during freezing: Effects on product morphology and drying behaviour

Vincenzo Massotti, Fiora Artusio, Antonello A. Barresi, Roberto Pisano *

Department of Applied Science and Technology, Politecnico di Torino, 24 corso Duca degli Abruzzi, IT, 10129, Torino, Italy

ARTICLE INFO

ABSTRACT

Freeze-drying of biopharmaceuticals is a crucial operation to increase their stability and shelf-life. Parenteral drug products are generally frozen in vials placed in contact with a temperature-controlled shelf. Uncontrolled nucleation is a source of batch heterogeneity, as nucleation occurs at different temperatures in vials frozen at different times. Heat released from a vial undergoing solidification may be transferred to neighbouring vials, impacting their thermal profiles and altering the distribution of the nucleation temperature and the freezing rate within the batch. This study characterised thermal coupling in interacting and non-interacting loading configurations. These estimations were used as input in a simple 1D mathematical model to assess the effect of thermal interactions on the freeze-dried product morphology. Thermal interactions strongly impacted the predicted nucleation temperature, especially for late-nucleating vials, and the freezing rate. The combined effect of thermal coupling on nucleation temperature and freezing rate resulted in different frozen product morphology. Heterogeneity within a batch of interacting vials was higher compared to non-interacting vials, leading to broader pore size and drying time distributions, in agreement with experimental data. The presented model provides insight into the thermal history of each vial of the batch during freezing, supporting the rational design of freezing processes.

1. Introduction

Freezing is a crucial operation in the biopharmaceutical industry, playing a key role in the manufacturing of freeze-dried drugs and the storage of vaccines, therapeutics, and biological samples. In recent years, it has been proposed that the optimal design of freezing processes should be grounded in the fundamental understanding of the underlying physical phenomena rather than relying on trial-and-error methods (Assegehegn et al., 2019; Capozzi and Pisano, 2018). This rational approach enables more precise control of product quality, as required by regulatory authorities.

During freezing, the product temperature is gradually lowered to achieve the solidification of the solution. This process takes place in two stages: the cooling phase, where water is cooled below its freezing point, followed by the solidification phase, during which the phase transition takes place. Solidification begins with a stochastic event called nucleation, which refers to the formation of the first stable ice nuclei. These nuclei lead to the formation of ice crystals that continue to grow until the entire solution is frozen. When vials containing a drug product undergo

freezing, the process conditions influence the ice crystals features, such as their number, size, and morphology. More specifically, low nucleation temperatures and fast freezing rates result in smaller ice crystals (Searles et al., 2001).

Due to the stochasticity of nucleation, the crystal populations differ from vial to vial in terms of ice crystal size, leading to a non-negligible source of batch heterogeneity. In the case of freeze-dried products, this feature determines the pore structure of the final product (Artusio et al., 2025; Hottot et al., 2007; Levin et al., 2021; Pisano et al., 2023), influencing the choice of the optimal operating parameters of both primary and secondary drying (Pisano et al., 2019; Searles et al., 2001). In particular, larger pores speed up ice sublimation as the resulting resistance to the vapour flow decreases. In contrast, the formation of smaller pores facilitates secondary drying since the larger surface area favours the desorption of water, reducing the residual moisture. Finally, the crystal/pore size is a critical parameter for the stability and recovery of the activity of enzymes/biomolecules (Cochran and Nail, 2009).

Pharmaceutical products are typically frozen at a cooling rate between 0.1 and 1°C min^{-1}. In these conditions, the ice crystal/pore size is

---

mainly determined by nucleation temperature (Searles et al., 2001) and the solid content of the solution (Košir et al., 2025), rather than by the cooling rate (Deck and Mazzotti, 2023). However, measuring the nucleation temperature of every vial of the batch to obtain the nucleation temperature distribution poses several experimental challenges. Temperature is generally monitored by thermocouples, but their presence is known to alter the nucleation events via heterogeneous nucleation (Searles et al., 2001). As an alternative, thermal imaging cameras could be used as non-invasive temperature sensors (Deck et al., 2024a), but they are not easily applicable because of loading constraints and the need for calibration.

Conversely, determining the nucleation time distribution can be achieved through video cameras, without the need for a complex setup. The nucleation temperature distribution can then be estimated from the nucleation time distribution, as proposed by Capozzi and Pisano (2018). When nucleation starts, the product shifts from a clear to an opaque appearance, making it possible to record the nucleation time of each vial in the batch through video cameras and to obtain the distribution within the batch. Knowing the cooling rate of selected vials monitored by thermocouples, it is possible to extrapolate the nucleation temperature from the corresponding nucleation time. However, this approach is accurate only in the absence of thermal coupling between neighbouring vials.

Due to the complexity of the involved phenomena and the difficulties related to the experimental approach, attention has been focused on computational tools. Several mathematical models have been proposed to describe the freezing step of aqueous solutions in vials, particularly focusing on the estimation of product temperature profiles and the prediction of ice crystal size. Hottot et al. applied the conductive heat transfer equation to obtain a 2D axisymmetric model of freezing in a vial (Hottot et al., 2006). Nakagawa et al. (Nakagawa et al., 2007; Nakagawa et al., 2011) simulated the freezing profiles of pharmaceutical formulations, taking into account the vial geometry and the freezing conditions. Being limited to the simulation of a single vial, these models give a detailed description of both axial and radial gradients experienced by the product. A semi-empirical model was also used to estimate the mean ice crystal sizes as a function of the freezing front rate and the axial thermal gradients. This modelling framework has also been adopted to predict the temperature profile of the outer wall of axially spinning vials during freezing and has been validated using experimental data obtained from an infrared camera (Nuytten et al., 2021). The dependence of ice crystal size on the freezing front rate and the axial gradients has been confirmed by the mechanistic model proposed by Arsiccio et al. (2017). Colucci et al. (2020) proposed a mathematical model to monitor the temporal evolution of the ice crystal size distribution during freezing by combining nucleation and crystal growth kinetics to a population balance equation. The impact of nucleation stochasticity and thermal gradients on the freezing process has been explored in the mechanistic freezing model proposed by Deck et al. (2024b). Thanks to the development of freezing models, it has also been possible to propose and validate a rational method to design the freezing phase (Arsiccio and Pisano, 2018). The impact of freezing conditions on ice crystal size and process efficiency was investigated to enable a Quality-by-Design (QbD) approach when selecting freezing conditions.

More recently, emphasis has been put on the role of thermal interactions occurring among vials during the freeze-drying process. Several studies reported that vials in denser arrangements exhibit longer drying times compared to less dense configurations (Ehlers et al., 2021a; Matejčíková and Rajniak, 2020; Matejčíková et al., 2022). The drying dynamics of vials is affected by the spacing among vials, particularly when rack systems are used to host the vials (Artusio et al., 2023; Ehlers et al., 2021b). A different phenomenon occurs during freezing as vials close to a vial that undergoes nucleation receive from this one an additional heat contribution due to the exothermic formation of ice (Deck et al., 2022; Pisano et al., 2024). Therefore, the early nucleating vials delay the nucleation events in the surrounding ones, further

complicating the comprehension of the freezing process. Under these conditions, also the extrapolation procedure used to estimate the nucleation temperature from the nucleation time becomes inaccurate, as the relationship between the two is not so straightforward. Pisano et al. (2024) reported that the extent of thermal interactions during the freezing phase can significantly alter the nucleation time distributions. More specifically, when thermal interactions among vials are present, the nucleation time distributions are bimodal, whereas they tend to be monomodal when interactions are negligible. Deck et al. (2024a) used infrared thermography to observe the effect of thermal interactions during freezing on the thermal profile of vials in different arrangements. Specifically, vials were arranged in a spaced rectangular matrix using a rack and in a compact hexagonal one to modulate the effect of thermal interactions between them. The increase in the extent of thermal interactions caused an increase in the nucleation temperature and a decrease in the solidification time, in addition to an increase in their variability. However, the consequences of these variations on the product morphology are still unclear.

Because of thermal interactions and the stochasticity intrinsic to nucleation, it is difficult to rigorously predict the temperature profiles of each vial of the batch during freezing, and most of the reported modelling approaches focused on the single-vial scale. Recently, a shelf-scale model including thermal interactions has been proposed by Deck et al. (2022) to understand the impact of freezing on stacked vials and batch heterogeneity. Being a 0D model, the presence of axial gradients is neglected, hence it is not possible to extract information about the product morphology in the vial. Nevertheless, the accurate quantification of the heat transferred through lateral walls following nucleation in adjacent vials is still challenging.

In this work, we derive a mathematical model of freezing that considers thermal interactions among adjacent vials. At first, the heat exchanged through the lateral walls of vials following nucleation events was experimentally estimated from the thermal profiles recorded by thermocouples. This information, together with the map of the nucleation times, was used as input to develop a simple 1D mathematical model, which solves an energy balance equation for the whole batch and predicts the thermal profile of each vial with limited computational time. Knowing the thermal profiles, the model extracted information on the nucleation temperature, the freezing rate and the frozen product morphology, which was compared with experimental data, i.e., micrographs of the cake structure. Finally, it evaluated the product resistance to the vapour flow and the drying time of each vial of the batch, giving a complete overview of the impact of the operating parameters on the quality attributes (and their heterogeneity in the batch) of a freeze-dried product. The model showed a good agreement with experimental tests carried out in different configurations to highlight the role of heat and mass transfer limitations.

2. Materials and methods

2.1. Materials

A 5 wt% sucrose and a 5 wt% mannitol and sucrose (1:1) (analytical grade, Merck, Italy) solution were prepared using water for injection (Fresenius Kabi, Italy) and filtered through a 0.2 μm filter (PVDF, Merck, Italy). Both the freezing and freeze-drying tests were performed using 2R ISO tubing vials (Soffieria Bertolini, Candiolo, Italy), having a volume of 4 mL, an inner diameter of 14 mm and an outer diameter of 16 mm. All the vials were filled with 2 mL of the solution, corresponding to a filling height of 14 mm.

2.2. Freezing tests

The results of freezing tests performed (in triplicate) in our previous work (Pisano et al., 2024) were used to estimate the heat transferred due to thermal interactions. A batch of unstoppered vials was filled with 2

mL of a 5 wt% sucrose solution and arranged in a hexagonal pattern within the freeze-dryer (REVO, Millrock Technology, Kingston, New York, USA). Two video cameras were placed inside the chamber to visualise the nucleation events inside a matrix of 10 × 20 vials. The thermal profile of three vials was monitored by placing three miniature thermocouples (T-type) at their centre bottom. Two thermocouples were placed in two vials in the central part of the batch, while the third one in a lateral position, as reported in Fig. 1 (a) and (b). A cooling ramp (0.5°C min⁻¹) was applied to cool down the shelf to –45°C (holding time = 20 min) and freeze the solution in the vials. Then, the frozen solution was thawed by heating the shelf to +25°C (3°C min⁻¹). The nucleation event inside each vial was identified thanks to a change in opacity of the liquid detected by two video cameras (frame acquisition rate = 5 fps). The nucleation time of each vial in the batch is therefore known and expressed as the time elapsed from the instant at which a reference vial containing a thermocouple reaches 0°C to the instant at which the vial nucleates, thus corresponding to the undercooling time of the vial. The same procedure was followed during the freeze-drying tests with the sucrose-mannitol solution to obtain the nucleation time distribution curves that served as input to the model.

2.3. Freeze-drying cycles

To evaluate the effect of thermal interactions on the product morphology, four freeze-drying cycles were performed with different loading conditions, as described in Table 1. In Test A and B, vials were frozen in interacting (dense hexagonal packing) and non-interacting (with filled vial surrounded by empty vials) loading conditions, respectively, and the same configuration was maintained for drying. In Test C vials frozen in an interacting configuration were then separated inserting empty vials before drying, while the opposite was done in Test D, removing the empty vials and arranging the filled ones into a dense packing. Since sucrose is highly sensitive to atmospheric humidity, a 1:1

Table 1
Summary of the loading conditions of vials in the different test cases.

Test case	Freezing configuration	Frozen vials	Drying configuration	Dried vials
A	dense packing	140	dense packing	140
B	filled vials separated by empty vials	30	filled vials separated by empty vials	30
C	dense packing	140	filled vials separated by empty vials	30
D	filled vials separated by empty vials	30	dense packing	30

formulation of sucrose and mannitol was used for the freeze-drying cycles to facilitate the freeze-dried product morphology characterisation. In all loading conditions, vials were placed in a hexagonal arrangement in contact with the temperature-controlled shelf. The experiments only involved the central vials of the batch so as to avoid edge effects. This was achieved loading the vials within a metal frame and using empty edge vials to shield the central ones. The nucleation time of each vial of the batch was recorded by video cameras, as previously detailed, and used as an input for the simulation of the corresponding experimental test. The number of monitored vials (and recorded nucleation events) is reported in Table 1. The product was frozen at –45°C with a 0.5°C min⁻¹ cooling ramp. Primary drying was performed at 10 Pa and –30°C, then temperature was increased to 30°C (0.2°C min⁻¹ ramp rate) to perform secondary drying for 14 h. Selected vials corresponding to early, average, and late nucleation times were sampled for microstructure analysis via Scanning Electron Microscopy (SEM, FEI, Quanta Inspect 200, Eindhoven, Netherlands). The freeze-dried cakes were cut along the axial direction, glued to the SEM stub, and metallised with a few nm-thick layer of Pt for SEM imaging. The reported data refers to the pore size of the dried cake in the central part of the sample. Assuming that the pores have an elliptical shape, the reported pore size refers to a circle that has the same area-to-perimeter ratio as the ellipse.

2.4. Determination of the overall equipment-to-product heat transfer coefficient during freezing (U_s) and drying (K_v)

The heat transfer coefficient between the equipment and the product during the freezing phase (U_s) was evaluated following the procedure detailed in Pisano et al. (2023). This approach is based on the quantification of the heat flow rate between the shelf and the vial bottom knowing the shelf and product temperature dynamics during the cooling phase.

The overall heat transfer coefficient between the equipment and the product during primary drying (K_v) was determined for each vial of the batch considering two configurations: densely packed vials and vials spaced by empty vials. Briefly, a gravimetric test was performed to evaluate the weight loss of each vial after a given sublimation time. K_v was calculated following the procedure detailed in Pisano et al. (2011). U_s and K_v are expressed in W m⁻² °C⁻¹ and are referred to the vial internal cross-sectional area.

2.5. Determination of the lateral heat transfer coefficient (K_s)

The heat transfer between neighbouring vials mainly occurs by conduction through the glass walls and by free convection with the air between the two vials. Assuming that the products in the two interacting vials are separated by a multilayered wall (glass of vial 1, air, and glass of vial 2), the overall lateral heat exchange coefficient K_s can be written as:

$$K_s = \left(\frac{t_g}{k_g} + \frac{1}{h_{air}} + \frac{t_g}{k_g} \right)^{-1}$$

(1)

where t_g is the thickness of the glass wall of the vials, k_g is the thermal
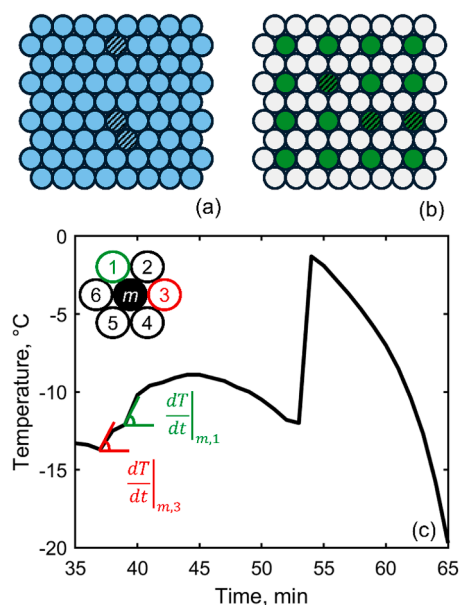
Fig. 1. Schematics of the arrangements of vials over the shelf. (a) Interacting configuration with filled vials (light blue) arranged in a dense hexagonal packing and (b) non-interacting with filled vials (green) spaced by empty vials (white). The presence of thermocouples is highlighted by the pattern fill. (c) Temperature evolution of the "m" vial during freezing, which nucleated after 53 min. The neighbouring vials (dense packing) nucleated after 38 min (vial 3) and 41 min (vial 1). The local change in the slope of the temperature profile was used to determine the thermal power received by the "m" vial. The schematic of the investigated vial arrangement where the "m" vial is equipped with thermocouples is shown in the inset.

conductivity of glass, and h_{air} is the heat transfer coefficient due to free convection with air. The terms in Eq. (1) are characterised by a high uncertainty due to two main reasons. At first, the close contact between two vials cannot be ensured during the process, since the relative position of the vials can vary due the vibration of the equipment, but eventually a further contribution along to the contact line should be considered. Secondly, h_{air}, calculated using empirical correlations (Pisano and Capozzi, 2017), depends on the temperature of the air between the two vials, which is difficult to monitor and varies due to the heat released during the phase change. For these reasons, the value of K_s was evaluated experimentally as a global heat exchange between neighbouring vials.

The heat exchanged due to thermal interactions was quantified by observing the effect of nucleation events occurring in adjacent vials on the thermal profiles recorded by thermocouples. When the solution in a neighbouring n vial nucleates, it causes a sudden increase in the temperature of the solution monitored by the thermocouple m. This increase was quantified by measuring the time derivative term $dT/dt|_{m,n}$ related to the heat transferred from the n to the m vial. This term was defined as the slope of the tangent line at the point corresponding to the nucleation event in the n vial. Knowing that the thermal power related to thermal interactions is transferred as sensible heat to the solution in vial m, K_s was determined calculating the rate of heat exchanged between the two vials following ice nucleation:

$$K_s A_s \left(T_{TC,m} - T_{eq,n} \right) = m_{sol}\, c_{p,sol} \frac{dT}{dt}\bigg|_{m,n} \tag{2}$$

where A_s is the lateral surface of the liquid/frozen solution, $T_{TC,m}$ is the temperature of the reference vial (see scheme in the inset of Fig. 1c) measured by the thermocouple, $T_{eq,n}$ is the temperature of the n neighbour vial at the time immediately after nucleation occurred (that is, the equilibrium temperature for ice crystallisation), m_{sol} is the mass of the solution in the vial, $c_{p,sol}$ is the specific heat capacity of the solution, and $dT/dt|_{m,n}$ is the temperature rise term previously described. The determination of $dT/dt|_{m,n}$ is shown for two cases in Fig. 1 (c). Since the m vial is in contact with six neighbouring ones, the lateral surface area A_s is taken equal to one-sixth of the total lateral surface area of the product. This procedure was applied to the dense packed loading configuration, as vials spaced by empty ones were not affected by the neighbouring nucleation events.

Previous results (Pisano et al., 2024) showed that the two loading configurations considered in the present work were those with maximum and minimum (null) interaction, respectively. Analysis of data confirmed that temperature interaction effects could be observed only with the compact loading, and thus K_s values were determined for this configuration, while for the case with empty vials separating the active vials the assumption of no interaction was correct.

2.6. Mathematical model for the freezing of interacting vials

A hexagonal matrix arrangement of vials is considered, where each vial is identified by the (i, j) coordinates, representing the row and column, respectively (see Fig. 2 (a)). During the freezing phase, the evolution of the product temperature in each vial of the batch is calculated by numerically solving $i \times j$ energy balance equations. A 1D modelling framework was established to take into account the thermal gradients along the vertical direction. The contributions to the following thermal balance equations are schematised in Fig. 2b:

$$\rho_{sol} c_{p,sol} \frac{\partial T}{\partial t} = \nabla \cdot (k_{sol} \nabla T) + \widehat{Q}_{int} + \widehat{Q}_c \tag{3}$$

where k_{sol} is the thermal conductivity of the solution, $\widehat{Q}_{int}$ is the specific rate of heat exchanged due to thermal interactions through the lateral wall, and $\widehat{Q}_c$ is the specific rate of heat released during crystallisation.
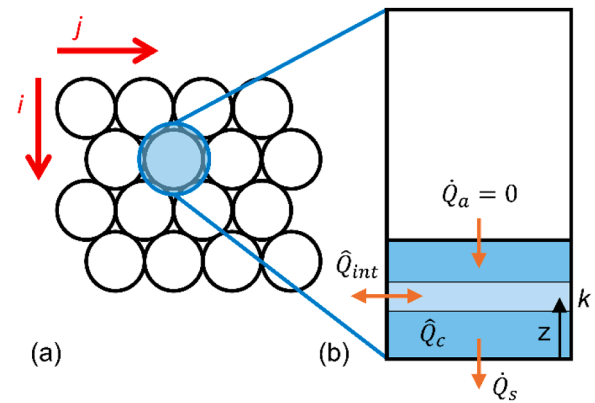

Fig. 2. Schematic of (a) the (i,j) vial position within the batch, (b) the contributions to the overall thermal balance in the (i, j) vial.

The heat exchange with the air at the top of the vial was neglected ($\dot{Q}_a = 0$), while the heat exchanged with the shelf is calculated as follows:

$$\dot{Q}_s = U_s A (T_s - T) \tag{4}$$

where U_s is the overall equipment-to-vial heat transfer coefficient, A is the cross-sectional area of the vial, T is the temperature of the product, and T_s is the temperature of the shelf, which varies as previously reported.

The specific heat $c_{p,sol}$, the thermal conductivity k_{sol} and the density ρ_{sol} are considered independent of temperature and are assumed to have a linear relationship with the composition of the solution:

$$c_{p,sol} = x_w c_{p,w} + x_i c_{p,i} + x_s c_{p,s} \tag{5}$$

$$k_{sol} = x_w k_w + x_i k_i + x_s k_s \tag{6}$$

$$\rho_{sol} = x_w \rho_w + x_i \rho_i + x_s \rho_s \tag{7}$$

where x, c_p, k and ρ are, respectively, the mass fraction, the specific heat capacity, the thermal conductivity, and the density of water (w), ice (i), and solutes (s). The properties of the different species are reported in Table 2.

To properly take into account axial thermal gradients, the liquid volume was discretised in K layers identified by the index k. Assuming that the mass density of water is constant with the temperature, the heat exchange between the layers mainly occurs by conduction. In order to simplify the calculations, the model neglects the presence of radial gradients. The validity of this assumption was then confirmed by SEM imaging, as the dried cake did not evidence a significant pore size distribution along the radial direction (see Fig. S4 in the Supporting Information).

The map of nucleation times determined experimentally, correlates the nucleation time to the position of each vial in the batch and is used as a model input to initiate the phase change in the corresponding simulated vials. During nucleation, the temperature of the product suddenly increases until it reaches the equilibrium temperature. This phenomenon is simulated by imposing the temperature equal to T_{eq} at the time

Table 2
Specific heat capacity, thermal conductivity, and density of water, ice, sucrose and mannitol (Arsiccio et al., 2017; Giauque and Stout, 1936; Green and Perry, 2008; Honig, 1953; Mojiri et al., 2018; Nakagawa et al., 2007; Singh and Medina, 1989).

	Water	Ice	Sucrose	Mannitol
c_p, J kg^{-1}°C^{-1}	4186	2108	1240	1312
k, W m^{-1}°C^{-1}	0.57	2.5	0.15	0.15
ρ, kg m^{-3}	1000	918	1590	1520

instant immediately after nucleation occurred. The value of T_{eq} depends on the solid content, which causes a depression in the freezing point:

$$T_{eq} = T_{eq}\big|_{pure\ water} - k_f n \qquad (8)$$

where k_f is the cryoscopic constant of water and n is the molality of the solution.

When the system reaches its equilibrium temperature, it tends to keep its temperature constant by releasing the thermal power $\hat{Q}_c$. Assuming that the heat is removed from the product as latent heat, the ice mass fraction at the time t can be defined as the fraction of latent heat of solidification removed from the product at the time t. At each time step, the ice mass fraction is calculated as the ratio between the integral of the net heat removed from the product ($\dot{Q}_{rem}$) and the latent heat of solidification:

$$x_i(t) = \frac{\int_{t_n}^{t} \dot{Q}_{rem} dt}{m_w \lambda} \qquad (9)$$

where t_n is the nucleation time, m_w is the mass of water, and λ is the latent heat of solidification of water.

The model solves the energy balance for the entire batch of vials visualised by video cameras (see Table 1 for batch size). The simulations started at the end of the cooling phase, i.e. when the average temperature of the product decreases below 0 °C for the first time. The temperature of the shelf was initialised at the value measured by the instrument at the end of the cooling phase and is lowered to –45 °C with a cooling ramp equal to 0.5 °C min^{-1}. The simulated time is equal to 100 min with a time step dt of 0.005 s, and vials were discretised in 10 layers along the vertical axis. The time step and the number of layers were selected verifying that the solution was independent of the chosen discretization. The differential equations were numerically solved using the explicit Euler method.

The model simulates the thermal history of the experimental batch, extracting information about the nucleation temperature T_n, the freezing front velocity v_f, and the thermal gradients θ_k. This information allows us to estimate the crystal size D_p using the mechanistic model developed by Arsiccio et al. (Arsiccio et al., 2017; 2019), which previous work demonstrated to give performances equivalent to more complex models including population balances (Harguindeguy et al., 2022). Since the heat is being removed by the shelf, the freezing front moves from the bottom to the top of the product, as confirmed by infrared thermography (Harguindeguy et al., 2022). The proposed correlation was modified to take into account the presence of thermal interactions:

$$D_{p,k} = \frac{4m\overline{\theta}_k v_{f,k} \gamma b}{\rho_i \, \overline{\theta}_k^{2/3} \left(m\overline{\theta}_k v_{f,k} \lambda - k_f \overline{\theta}_k A s_{layer} \sum \overline{\theta}_k - K_s A_s \Delta T s_{layer} \sum \overline{\theta}_k \right)} \qquad (10)$$

where γ is related to the enthalpy change due to surface generation, b takes into account the crystal habit, and s_{layer} is the thickness of the frozen layer. Further details on the mathematical formulation of Eq. (10) are reported in the Supporting Information (S1).

Knowing the pore size distribution, the resistance to the vapour flow R_p is calculated as follows:

$$R_p = \frac{3}{2} \frac{\tau^2}{\varepsilon} \frac{s}{D_p} \sqrt{\frac{\pi R T}{2 M_w}} \qquad (11)$$

where τ and ε are the tortuosity and the porosity of the dried cake, respectively, s is the thickness of the dried layer, D_p is the average pore size in the vial, R is the ideal gas constant, T is the temperature of the product during primary drying and M_w is the molecular weight of water. The ratio τ^2/ε was taken equal to 0.225 as reported in previous studies (Capozzi and Pisano, 2018). Given the distribution of the average R_p in the batch, the drying times were estimated by using the 1D mathematical model proposed by Velardi and Barresi (2008). The parameters used

as input for the model are listed in Table 3.

3. Results and discussion

A 1D mathematical modelling framework was developed to understand the thermal behaviour of a batch of vials during the freezing phase. To properly take into account thermal interactions between adjacent vials, experiments were carried out to quantify the lateral heat transfer coefficient. We compared the model outcomes, i.e. nucleation temperature, pore size, and drying time distributions for the entire batch of vials considering two loading configurations to identify the impact of the thermal history experienced by the product in vials on the freeze-dried product quality attributes. Vials were loaded in a hexagonal arrangement over the temperature-controlled shelf. A full load configuration was first considered to maximise the extent of thermal interactions among adjacent vials during the freezing phase (interacting configuration). Alternatively, a partial load configuration was investigated where filled vials were spaced with empty vials to avoid thermal interactions during the freezing phase (non-interacting configuration). Additional tests with inverted configurations during the drying phase were carried out to highlight the role of heat and mass transfer limitations.

3.1. Evaluation of interaction in different loading configurations

In our previous paper (Pisano et al., 2024), vials were placed in different arrangements over the shelf to modulate their interactions and observe their effect on the nucleation time distribution. The correlation between the nucleation times of adjacent vials was evaluated using the global Moran's index. Among those configurations, the more and the less interacting were chosen as reference in this work. When vials were placed in a dense hexagonal arrangement, i.e., each vial was in contact with six neighbouring ones, thermal interactions strongly impacted the nucleation time distribution. Since vials are free to interact and their interaction resulted to be maximised in this loading configuration, it will be referred to as interacting configuration. On the contrary, the interactions between vials were completely suppressed when filled vials were spaced by empty ones. This arrangement will be named non-interacting configuration. A schematic of these configurations is reported in Fig. 1 (a) and (b). In the interacting configuration, vials that undergo an early nucleation delay the nucleation in the neighbouring ones, causing an increase in the average nucleation times and broadening their distribution. On the contrary, when vials do not interact, the distribution is narrower and centred around lower nucleation times. These behaviours were observed for all the formulations and in all test cases. The cumulative and relative distribution functions of nucleation times, both for sucrose and sucrose-mannitol solutions, are reported in the Supporting Information (S3).

Thermal interactions occurring during freezing are supposed to affect the product morphology, since they have an impact on both nucleation temperature and freezing rates (Deck et al., 2024a). The need to separate the vials to suppress thermal interactions may alter the heat

Table 3
Numerical values of the parameters used in the model.

	Interacting configuration	Non-interacting configuration
U_s, W m^{-2}°C^{-1}	55	75
$T_s(t = 0)$,°C	–8.8	–6.5
$T(t = 0)$,°C	0	0
γb, J °C$^{2/3}$ m$^{-8/3}$	6.2×10^5	9.3×10^5
τ^2/ε, -	0.225	0.225
K_v, W m^{-2}°C^{-1}	17	39
R, J mol^{-1}°C^{-1}	8.314	8.314
M_w, g mol^{-1}	18	18
A, m^2	1.54×10^{-4}	1.54×10^{-4}
A_s, m^2	1.03×10^{-4}	1.03×10^{-4}

supplied during drying (Ehlers et al., 2021a; Matejčíková and Rajniak, 2020; Matejčíková et al., 2022), making it difficult to determine whether the process is slowed down by heat or mass transport. To better understand the predominant phenomenon, vials were freeze-dried in different loading conditions, as listed in Table 1, where the different loading configurations were switched between the two phases of the process.

3.2. Quantification of the heat transfer originated by thermal interactions

Nucleation events occurring within adjacent vials can lead to unexpected changes in the slope of the product temperature profile measured by thermocouples, as shown in Fig. 1 (c) and can be employed to quantify the thermal interaction. The lateral heat transfer coefficient governing the heat received by a vial because of exothermal nucleation events occurring in adjacent vials can be determined using Eq. (2). Theoretically, the described configuration would allow the identification of eighteen nucleation events, i.e., six events per thermocouple, and three thermocouples. However, the actual number of nucleation events identifiable as variations in the thermal profile slope of a neighbouring vial may be smaller, as a consequence of multiple nucleation events co-occurring, resulting in cumulative effects, or due to loose contact. Significant variability was also observed in the estimated value, which may be due to variability in the contact among the vials, which can vary over time due to the vibrations of the equipment. Thus, distinguishing the effects of individual vials can become challenging. The value of the measured heat transfer coefficient K_s was in the range of 7.28 and 161.50 W $°C^{-1}$ m^{-2}, with an average value of 67.18 W $°C^{-1}$ m^{-2}. Despite evidencing a high variability, the average value has the same order of magnitude of estimations made in previous works (Deck et al., 2022, 2024a). In a configuration where vials were placed in a rectangular arrangement with an air gap between them, K_s variable between 10 and 45 W $°C^{-1}$ m^{-2} has been reported.

3.3. Impact of the vial thermal coupling on temperature profiles and freezing rates

To evaluate the effect of the vial thermal coupling on the product temperature profile, the value of K_s was varied between the minimum, average, and maximum values previously reported. At this stage, due to the difficulties in evaluating the K_s for each vial, it was assumed to be uniform within the batch. A future development could involve the stochasticity of K_s in the range reported to simulate the behaviour of a real batch. The average value represents the most likely behaviour of the system, while the minimum and the maximum values were used to determine the uncertainty associated to K_s. To estimate the impact of neglecting thermal interactions when predicting the thermal evolution of the product, an additional case with K_s equal to 0 was investigated. Fig. 3 compares the thermal profiles recorded by thermocouples with those of the bottom layer of the corresponding simulated vial. Referring to average K_s, the model showed in general a good agreement with the experimental results, reproducing the increase in temperature due to nucleation events in adjacent vials with sufficient accuracy. Fig. 3 also shows how the predicted temperature profile modifies changing the K_s value. It can be noted that some (or part) of the experimental curves deviated from the prediction based on the average K_s value because of the different inter-vial contact. Thus, the extent of the thermal interactions may change from vial to vial (and its exact value is unpredictable) and may also vary during the process.

The comparison among the different curves highlights that the vial thermal coupling can significantly affect the estimation of the nucleation temperature. This is evident in vials where ice nucleation was delayed by previous nucleation in neighbouring ones. These vials may exhibit a pronounced deviation from the expected behaviour (see an example in Fig. 3 (a)), resulting in an estimation error as high as 10°C if thermal interactions are not considered. The accuracy of this estimation
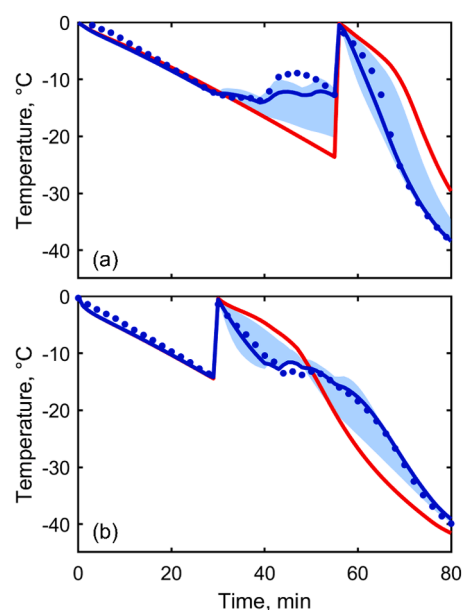

Fig. 3. Comparison of the product temperature profile (blue circles) recorded by thermocouples (a) TC1 and (b) TC2 with those predicted by the model in case of interacting vials (blue curves), and in case of neglected interactions (K_s=0, red curves). The light blue area refers to the uncertainty on the estimation of K_s. Freezing test; sucrose solution.

improves by taking into account thermal coupling, and a good agreement is reached considering the average K_s value. In the case shown in Fig. 3 (b), where nucleation was unaffected by surrounding vials, the estimation of the nucleation temperature was independent of the thermal coupling extent. However, the successive temperature profile was affected by the later nucleation events in the surrounding vials.

Thermal interactions were also responsible for a variation in the freezing rate, as they contribute to the dissipation of the latent heat during solidification. The values of the freezing front rate were calculated as described by Nakagawa et al. (2007) and are summarised in Table 4. Details on the evaluation of this physical quantity are reported in the Supporting Information (S2). As expected, the freezing front progressed more rapidly as vial thermal coupling increased. Similarly to the previous case, the effect of thermal interaction on the freezing rate differed between vials that did or did not experience the delay caused by the interaction. In the case of unaffected vials, i.e., TC2, the phase change occurred at a higher shelf temperature, resulting in a lower contribution from $\dot{Q}_s$. Consequently, the freezing front rate resulted three times higher when K_s was varied from the minimum to the maximum value. On the contrary, the contribution from $\dot{Q}_s$ was greater when vials were affected by delayed nucleation, and the maximum increase in the freezing front velocity was only approximately 60 % when the interaction was increased from the minimum to the maximum extent.

The model was then used to simulate the experimental conditions of the freeze-drying cycles A and B. The average K_s estimated from these tests showed a good agreement with that previously obtained in the freezing tests; therefore, it was used to represent the interactions arising

Table 4
Freezing front rate ($\times 10^{-5}$ m s^{-1}) of the product in the vials monitored by TC1 and TC2 as a function of the K_s used in the simulations.

	$v_{f,1}$	$v_{f,2}$
Neglected	4.29	1.49
$K_{s,min}$	4.31	1.74
$K_{s,av}$	5.27	3.43
$K_{s,max}$	7.64	5.65

in the interacting configuration. Fig. 4 reports the comparison between the thermal profiles computed by the model and those recorded by thermocouples. Also, in this case, the model showed a good agreement with the experimental results, correctly describing the behaviour of the sucrose-mannitol solution during freezing.

3.4. Evaluating nucleation temperature and freezing front variability in response to thermal coupling: a comparison between interacting and non-interacting loading configurations

The calculation of the nucleation temperature (T_n) and freezing front velocity (v_f) was extended to the entire batch of vials in freeze-drying Tests A and B by extracting these values from the simulated temperature profiles. To assess the effect of thermal coupling, the results were compared with those of the non-interacting configuration. An example of these results is given in Figs. 5 and 6, showing the cumulative distribution functions of T_n and v_f. The distributions corresponding to the different case studies are reported in the Supporting Information (S3).

Fig. 5 reports the cumulative distribution functions of T_n. The curves corresponding to Test A (blue curve) and Test B (green curve) highlight that the delay in the nucleation introduced by thermal interactions lowered T_n and increased its variability within the batch. More specifically, the average value decreased from –13.5 to –17.6 °C, while the standard deviation increased from 1.5 to 2.7 °C. When interactions were present, the stochasticity of nucleation overlaps with that introduced by the interactions, increasing the variability in the distribution of T_n.

Simulations with a higher value of K_s caused the shift of the uncertainty area towards higher temperatures and a reduced variability of the distribution. Even if thermal interactions delayed nucleation events, the associated degree of supercooling of the solution was reduced. These results confirm the good estimation made by the model, as a similar trend is observed in the experiments reported by Deck et al. (2024a).

Finally, the comparison with the red curve highlights the importance of considering thermal interactions. It is important to note that this case refers to a scenario in which thermal interactions are present, but they are not taken into account. When thermal interactions were neglected, we observed a difference in the median value of about 5 °C, in addition
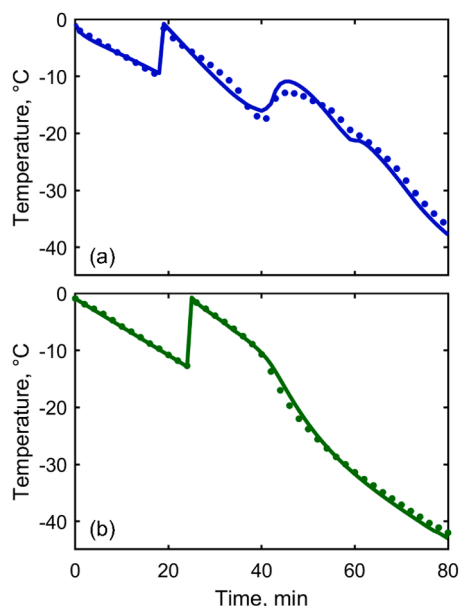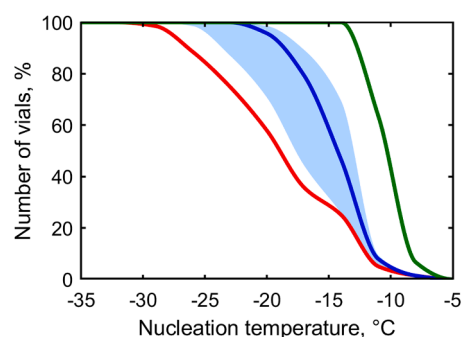
Fig. 5. Cumulative distribution functions of the nucleation temperature in case of interacting configuration (Test A, blue curve), non-interacting configuration (Test B, green curve), and the configuration with neglected interactions ($K_s=0$, red curve). The light blue area refers to the uncertainty on the estimation of K_s.

Fig. 6. Cumulative distribution functions of the freezing front rate in case of interacting configuration (Test A, blue curve), non-interacting configuration (Test B, green curve), and the configuration with neglected interactions ($K_s=0$, red curve). The light blue area refers to the uncertainty on the estimation of K_s.

to an overestimation of the variability of the distribution.

The model suggested a similar trend for the freezing front rate (see Fig. 6), with the freezing advancing more rapidly as the value of K_s was increased. In the case of the non-interacting configuration, v_f was lower and uniformly distributed within the batch. In this configuration, the only contribution to the dissipation of the latent heat of solidification was $\dot{Q}_s$, which affected all the vials to the same extent. As concerns the prediction for the interacting case, the addition of $\widehat{Q}_{int}$ led to an increase in the freezing rate from approximately 6×10^{-6} to 20×10^{-6} m s^{-1}.

In contrast to the observations for T_n, the increase in the extent of thermal interaction is associated with greater v_f variability. This result may be attributed to the different impacts of $\widehat{Q}_{int}$ and $\dot{Q}_s$ on the phase change. Even when the extent of interaction is high, its impact can be mitigated if $\dot{Q}_s$ prevails, and the resulting acceleration of the freezing front has a different extent within the batch. The results of the model are well supported by the experimental findings by Deck et al. (2024a). In their work, the authors reported a decrease in the solidification time, i. e., an increase in the freezing front rate, with the increase in the extent of thermal interaction.

3.5. Impact of thermal interactions on frozen product morphology

Previous results have evidenced the effect of thermal interaction on the distribution of nucleation temperature. Nucleation temperature is known to affect the frozen product morphology, as it determines the ice crystal size. On the other hand, thermal coupling is also responsible for the increase in the freezing front rate, the variability of which increases with the extent of interaction and, thus, has an opposite effect on the ice crystal size. To better clarify whether the product morphology is more

Fig. 4. Comparison between the thermal profiles predicted by the model (solid line) and those registered by thermocouples (dotted line) in case of (a) interacting (blue curve) and (b) non-interacting (green curve) configuration during the freezing step of Tests A and B, respectively. The tests were performed using a sucrose-mannitol solution.
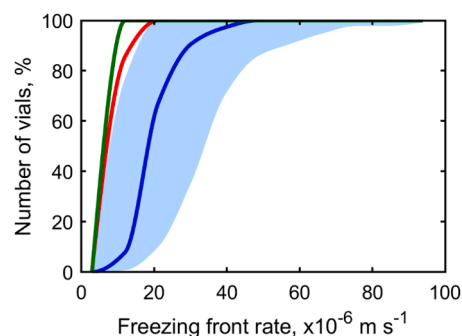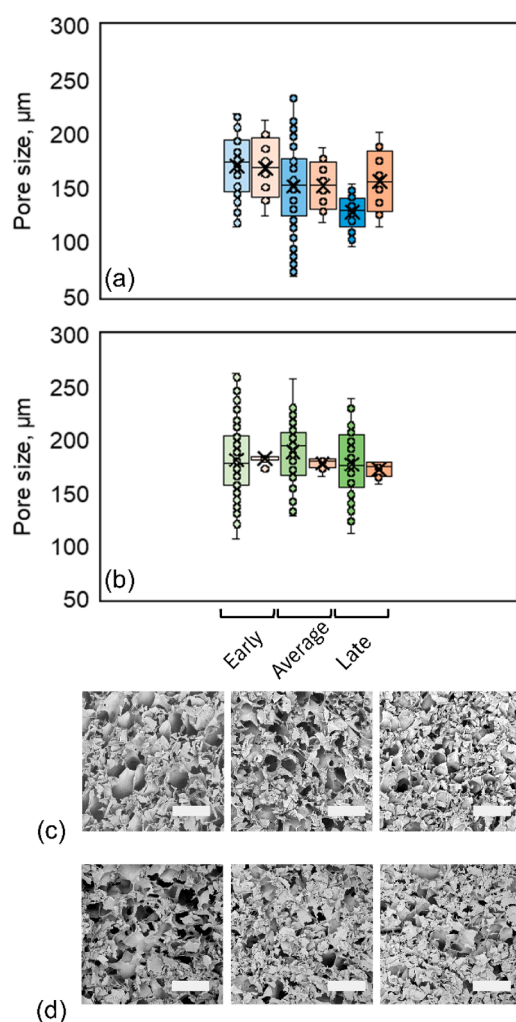
influenced by T_n or v_f, a mechanistic model (Arsiccio et al., 2017), whose parameters were determined by fitting using SEM imaging of the cake structure, was used to estimate the average pore size of the product. To estimate the heterogeneity in the product morphology within the batch, the average pore size in three vials nucleating at different time instants in the batch, i.e., early, average and late, was measured using SEM and reported in Fig. 7.

When thermal interactions were present (Fig. 7 (a)), the average pore size decreased from approximately 170 to 130 μm from early to late freezing vials. The freezing rate of the early nucleating vial was lower than that of the late ones, leading to the formation of larger crystals at the beginning of the freezing process and smaller ones at the end. On the contrary, for the non-interacting configuration (Fig. 7 (b)), the pore size was very uniform, with the mean value that was quite constant over time at approximately 180 μm.

Eq. (10) expresses the pore diameter as a function of the freezing front rate v_f and the axial thermal gradients θ_k. As previously reported, it requires the fitting of a parameter, namely γb, which is influenced by both freezing conditions and formulation (Arsiccio et al., 2017).

Therefore, the measures of the pore size were used to fit the parameter for the interacting and the non-interacting configurations. The values of the fitted parameters used in the model are reported in Table 3. The comparison between the dispersion of the measured pore size and the axial distribution computed by the model is reported in Fig. 7. In both cases, the model fairly reproduced the behaviour of the pore size over time, predicting the gradual reduction of its mean value for the interacting configuration and the high homogeneity of the non-interacting one. In the first case, it predicted a pore size that decreases from approximately 170 to 155 μm, while in the second one, a mean value of about 175 μm. The distributions of the pore size measured by SEM imaging showed a wider distribution compared to the model predictions due to the stochasticity of the phenomenon. However, the model gave a good estimation of the average pore size of the selected samples. In the case of the non-interacting configuration, the freezing conditions were very homogeneous due to the absence of thermal interactions. This leads to a very uniform pore size, that caused the collapse of the distribution on the average value.
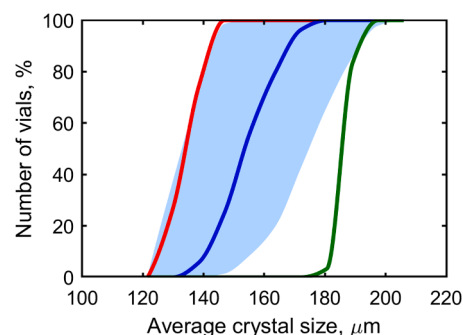
The model and Eq. (10) were then used to estimate the distribution of D_p within the batch. The cumulative distribution functions of D_p are reported in Fig. 8.

For the non-interacting configuration, the predicted ice crystal size was slightly higher than the interacting one, with a median value of 185 μm. The high nucleation temperature and the lower freezing rates led to the formation of larger crystals. The absence of thermal interactions led to a very low variability in the product morphology.

According to the trend of the nucleation temperature distribution, for the interacting case study, the estimated ice crystal size increased with the values of the K_s considered, with the median value that increases from 130 to 175 μm. However, the heterogeneity of the freezing front rate resulted in a wider distribution of crystal size, whose variability, in this case as well, increased with the K_s considered. These results suggested that the nucleation temperature mainly influenced the average pore size, as higher nucleation temperature led to the formation of larger crystals. On the other side, the higher variability of the freezing front rate affected the variability of crystal size, leading to a less uniform product morphology within the batch. The comparison with the case of K_s equal to zero showed that neglecting the presence of thermal interactions would result in an underestimation of the average crystal size and its variability within the batch.

3.6. Impact of thermal interactions on freeze-drying process performance

The results of the simulations suggested that thermal interactions alter the pore size distribution within the batch, decreasing the average value, and broaden its distribution. This result may also affect the primary drying, as the process should be slowed down by the higher resistance to the vapour flow. However, as previously discussed, the

Fig. 7. Comparison between the pore size predicted by the model (orange bars) and the pore size measured using SEM imaging for (a) interacting (blue bars) and (b) non-interacting (green bars) configuration. The solid line inside the boxes indicates the median value, while the cross refers to the average value. The bottom and the top edges of the boxes represent the first and the third quartile, respectively, and the whiskers represent the minimum and maximum values of the dispersion. Panels (c) and (d) report SEM micrographs of the dried cake of the product in the interacting and in the non-interacting configuration, respectively. From left to right: early, average and late nucleating vials.

Fig. 8. Cumulative distribution functions of the mean crystal size in case of interacting configuration (Test A, blue curve), non-interacting configuration (Test B, green curve), and the configuration with neglected interactions (K_s=0, red curve). The light blue area refers to the uncertainty on the estimation of K_s.

need to separate the vials with empty vials may alter the heat supplied during drying, making it difficult to determine whether the process is slowed down by heat or mass transport. To better understand this phenomenon, two additional freeze-drying cycles with different packing configurations were performed. Specifically, in Test C vials frozen in an interacting configuration (as Test A) were separated by empty ones before drying, while the opposite was done in Test D (see Table 1). The comparison between the four configurations was made in term of the endpoint of primary drying, evaluated as the offset of the Pirani/Baratron pressure signal. These results are shown in Fig. 9.

As reported by Ehlers et al. (2021a) and Matejčíková et al. (Matejčíková and Rajniak, 2020; Matejčíková et al., 2022), the shelf to vial heat transfer coefficient may depend on type and density of packing and is affected by the presence of empty vials. To confirm this phenomenon, K_v was measured for both configurations, and our results confirmed the experimental finding of previous authors. For the compact loading, K_v was equal to 17 W m$^{-2\circ}$C^{-1}, while it increased to 39 W m$^{-2\circ}$C^{-1} when empty vials were inserted to surround the active ones. This effect caused a difference of about 25 h in drying times between vials that are dried in a dense packing configuration (Test A and D) compared to those with enhanced heat transfer (Test B and C).

The drying times in Test A and D were approximately 67 and 65 h. In case of compact loading during drying, the process was slowed down by lower heat transfer from the shelf, and the difference in morphology showed only a small effect on the drying time. Test B and C showed a drying time of approximately 40 and 46 h, respectively. In these cases, the heat flux from the shelf was significantly higher because the empty vials that surround the active vials increase the effective heat transfer coefficient. Apart from a contribution from radiation, due to a change in view factor, this increase was reasonably determined by the higher temperature reached by the empty vials (in absence of the sinking effect generated by the ice sublimation). As a result, the boundary condition of the active vial changed due to the increased heat flow passing through the vial wall. The difference in the drying time between Test A and C (or between D and B) confirmed that the process in normal conditions was under heat transfer control, thus structure and mass transfer resistance had a small effect. When the heat exchange is more efficient, as in Test B and C, mass transfer resistance becomes more relevant, and differences in the structure have a stronger impact on the drying times. A 15 % difference in the drying time was observed in these cases. It must be noted the cake resistance is not expected to be very high in the cases considered, reasonably reproducing common cases in the pharmaceutical industry where concentration and filling height are generally set at a low value to avoid problems during drying. However, filling height up to 20 mm, and much higher solid fractions, are not rare, and in these cases thermal interactions and structure effects on drying would be stronger.

The distributions of the average pore size were converted into the distribution of the resistance to the vapour flow of the batch of vials using Eq. (11). These distributions were used to obtain an estimation of the drying times (summarised in Table 5).
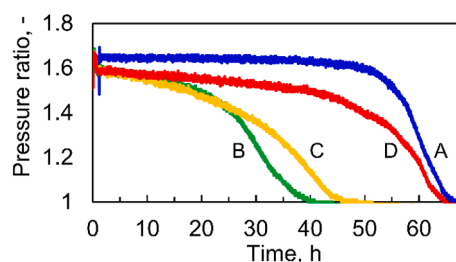
Table 5
Estimation of the drying times for Tests A-D made by the mathematical model.

	R_p, m s^{-1}	Drying time, h	Variability, h
Test A	$7.97 \times 10^3 - 1.86 \times 10^4$	50.7	0.7
Test B	$9.96 \times 10^3 - 1.19 \times 10^4$	24.9	0.4
Test C	$8.44 \times 10^3 - 1.86 \times 10^4$	25.9	0.8
Test D	$1.09 \times 10^4 - 1.32 \times 10^4$	49.9	0.4

The estimations of the model were in good agreement with the experimental results, giving a qualitative estimation of the onset of the Pirani/Baratron pressure signal. In case of interacting freezing, i.e., Test A and C, the variability of the estimation was slightly higher than the case of non-interacting freezing. This result may be attributed to heterogeneity in the product morphology caused by thermal interactions. In the other cases, the increase in the heat exchanged with the shelf led to a decrease in the drying times.

4. Conclusions

In this work, mathematical modelling was used to assess the impact of thermal interactions during freezing on the quality attributes of freeze-dried products. The heat released during the formation of ice in a vial influences the neighbouring ones, delaying their nucleation and affecting their thermal profile. The comparison with a non-interacting configuration showed that thermal interactions led to a decrease in the nucleation temperature and to a broader distribution. Moreover, this phenomenon impacted the freezing rate, which increased or decreased depending on the conditions of the surrounding vials. These deviations from the expected values cannot be neglected to estimate the morphology of the freeze-dried products correctly.

The mathematical model developed in this study accurately described the thermal history of products frozen in vial and their resulting morphology. Compared to the non-interacting configuration, thermal interactions decreased the pore size, and increased its variability within the batch, causing higher heterogeneity in the final product. This aspect did not significantly impact the drying times, which were comparable to those required by the non-interacting configurations. However, a limited impact was observed, as batches characterised by a higher resistance to the vapour flow exhibited higher drying times. While this effect was limited in the condition investigated in this work, it is expected to become more relevant where higher filling volumes or solid content are required. The model outputs showed good agreement with experimental results considering various case studies, where different conditions of interaction during both freezing and drying were considered. The results of this study emphasise the importance of considering thermal interactions in the design and optimisation of freeze-drying processes to improve the quality and consistency of freeze-dried products. By incorporating thermal interactions into a mathematical model, this research provides a comprehensive framework to predict key quality attributes, such as crystal size and drying times, thus facilitating the use of a Quality-by-Design (QbD) approach in freeze-drying.

CRediT authorship contribution statement

Vincenzo Massotti: Writing – original draft, Validation, Investigation, Formal analysis, Data curation, Conceptualization. **Fiora Artusio:** Writing – review & editing, Writing – original draft, Supervision, Investigation, Formal analysis, Data curation, Conceptualization. **Antonello A. Barresi:** Writing – review & editing, Supervision, Methodology. **Roberto Pisano:** Writing – review & editing, Supervision, Resources, Project administration, Methodology, Investigation, Funding acquisition, Data curation, Conceptualization.

Fig. 9. Pirani/Baratron pressure ratio in Test A (blue curve), Test B (green curve), Test C (yellow curve), and Test D (red curve).

Supplementary materials

Supplementary material associated with this article can be found, in the online version, at doi:10.1016/j.ejps.2025.107112.

Data availability

Data will be made available on request.

References

Arsiccio, A., Barresi, A.A., Pisano, R., 2017. Prediction of ice crystal size distribution after freezing of pharmaceutical solutions. Cryst. Growth Des. 17 (9), 4573–4581. https://doi.org/10.1021/acs.cgd.7b00319.

Arsiccio, A., Pisano, R., 2018. Application of the quality by design approach to the freezing step of freeze-drying: building the design space. J. Pharm. Sci. 107 (6), 1586–1596. https://doi.org/10.1016/j.xphs.2018.02.003.

Arsiccio, A., Sparavigna, A.C., Pisano, R., Barresi, A.A., 2019. Measuring and predicting pore size distribution of freeze-dried solutions. Drying Technol. 37 (4), 435–447. https://doi.org/10.1080/07373937.2018.1430042.

Artusio, F., Adami, M., Barresi, A.A., Fissore, D., Frare, M.C., Udrescu, C.I., et al., 2023. The freeze-drying of pharmaceuticals in vials nested in a rack system—part II: primary drying behaviour. Pharm. 15 (11), 2570. https://doi.org/10.3390/pharmaceutics15112570.

Artusio, F., Pisano, R., Massotti, V., 2025. Using rack systems to reduce thermal interactions between vials during freezing. Eur. Pharm. Rev. 30 (1), 41–45. Available online at: https://www.europeanpharmaceuticalreview.com/article/231260/enhancing-freeze-drying-uniformity-in-pharmaceuticals-using-rack-systems/.

Assegehegn, G., Brito-de la Fuente, E., Franco, J.M., Gallegos, C., 2019. The importance of understanding the freezing step and its impact on freeze-drying process performance. J. Pharm. Sci. 108 (4), 1378–1395. https://doi.org/10.1016/j.xphs.2018.11.039.

Capozzi, L.C., Pisano, R., 2018. Looking inside the 'black box': freezing engineering to ensure the quality of freeze-dried biopharmaceuticals. Eur. J. Pharm. Biopharm. 129 (1), 58–65. https://doi.org/10.1016/j.ejpb.2018.05.020.

Cochran, T., Nail, S.L., 2009. Ice nucleation temperature influences recovery of activity of a model protein after freeze drying. J. Pharm. Sci. 98 (9), 3495–3498. https://doi.org/10.1002/jps.21815.

Colucci, D., Fissore, D., Barresi, A.A., Braatz, R.D., 2020. A new mathematical model for monitoring the temporal evolution of the ice crystal size distribution during freezing in pharmaceutical solutions. Eur. J. Pharm. BioPharm. 148 (1), 148–159. https://doi.org/10.1016/j.ejpb.2020.01.004.

Deck, L.T., Ferru, N., Košir, A., Mazzotti, M., 2024a. Visualizing and understanding batch heterogeneity during freeze-drying using shelf-scale infrared thermography. Ind. Eng. Chem. Res. 63 (1), 16335–16346. https://doi.org/10.1021/acs.iecr.4c02215.

Deck, L.T., Košir, A., Mazzotti, M., 2024b. Modeling the freezing process of aqueous solutions considering thermal gradients and stochastic ice nucleation. Chem. Eng. J. 483 (1), 148660. https://doi.org/10.1016/j.cej.2024.148660.

Deck, L.T., Mazzotti, M., 2023. Characterizing and measuring the ice nucleation kinetics of aqueous solutions in vials. Chem. Eng. Sci. 272 (1), 118531. https://doi.org/10.1016/j.ces.2023.118531.

Deck, L.T., Ochsenbein, D.R., Mazzotti, M., 2022. Stochastic shelf-scale modeling framework for the freezing stage in freeze-drying processes. Int. J. Pharm. 613 (1), 121276. https://doi.org/10.1016/j.ijpharm.2021.121276.

Ehlers, S., Schroeder, R., Friess, W., 2021a. Trouble with the neighbor during freeze-drying: rivalry about energy. J. Pharm. Sci. 110 (3), 1219–1226. https://doi.org/10.1016/j.xphs.2020.10.024.

Ehlers, S., Schroeder, R., Friess, W., 2021b. Process optimization and transfer of freeze-drying in nested vial systems. Eur. J. Pharm. BioPharm. 159 (1), 143–150. https://doi.org/10.1016/j.ejpb.2021.01.002.

Giauque, W.F., Stout, J.W., 1936. The entropy of water and the third law of thermodynamics. The heat capacity of ice from 15 to 273 °K. J. Am. Chem. Soc. 58 (5), 1144–1150.

Green, D.W., Perry, R.H, 2008. Perry's Chemical Engineers' Handbook, 8th Ed. McGraw-Hill, New York.

Harguindeguy, M., Stratta, L., Fissore, D., Pisano, R., 2022. Combining mathematical modeling and thermal infrared data in the freezing of pharmaceutical liquid formulations. Ind. Eng. Chem. Res. 61 (12), 4379–4389. https://doi.org/10.1021/acs.iecr.1c04595.

Honig, P., 1953. Physical Properties of Sucrose, 1st Ed. Elsevier, New York.

Hottot, A., Peczalski, R., Vessot, S., Andrieu, J., 2006. Freeze-drying of pharmaceutical proteins in vials: modeling of freezing and sublimation steps. Drying Technol. 24 (5), 561–570. https://doi.org/10.1080/07373930600626388.

Hottot, A., Vessot, S., Andrieu, J., 2007. Freeze drying of pharmaceuticals in vials: influence of freezing protocol and sample configuration on ice morphology and freeze-dried cake texture. Chem. Eng. Process. 46 (7), 666–674. https://doi.org/10.1016/j.cep.2006.09.003.

Košir, A., Artusio, F., Deck, L.T., Pisano, R., Mazzotti, M., 2025. The impact of process parameters on the lyophilized porous micro-structure: a case study of dextran. J. Pharm. Sci. 114 (1), 1434–1443. https://doi.org/10.1016/j.xphs.2024.12.020.

Levin, P., Meunier, V., Kessler, U., Heinrich, S., 2021. Influence of freezing parameters on the formation of internal porous structure and its impact on freeze-drying kinetics. Processes 9 (8), 1–14. https://doi.org/10.3390/pr9081273, 1273.

Matejčíková, A., Rajniak, P., 2020. Impact of packing density on primary drying rate. Acta Chimica Slovaca 13 (2), 30–37. https://doi.org/10.2478/acs-2020-0021.

Matejčíková, A., Tichý, E., Rajniak, P., 2022. Experimental investigation of inhomogeneities of primary drying during lyophilization: impact of the vials packing density. J. Drug Delivery Sci. Technol. 74 (1), 103550. https://doi.org/10.1016/j.jddst.2022.103550.

Mojiri, A., Grbac, N., Bourke, B., Rosengarten, G., 2018. D-mannitol for medium temperature thermal energy storage. Solar Energy Mater. Solar Cells 176 (1), 150–156. https://doi.org/10.1016/j.solmat.2017.11.028.

Nakagawa, K., Hottot, A., Vessot, S., Andrieu, J., 2011. Modeling of freezing step during vial freeze-drying of pharmaceuticals- influence of nucleation temperature on primary drying rate. Asia-Pac. J. Chem. Eng. 6 (2), 288–293. https://doi.org/10.1002/apj.424.

Nakagawa, K., Hottot, B., Vessot, S., Andrieu, J., 2007. Modeling of freezing step during freeze-drying of drugs in vials. AIChE J. 53 (5), 1362–1372. https://doi.org/10.1002/aic.11147.

Nuytten, G., Revatta, S.R., Van Bockstal, P.J., Kumar, A., Lammens, J., Leys, L., et al., 2021. Development and application of a mechanistic cooling and freezing model of the spin freezing step within the framework of continuous freeze-drying. Pharm. 13 (12), 2076. https://doi.org/10.3390/pharmaceutics13122076.

Pisano, R., Arsiccio, A., Nakagawa, K., Barresi, A.A., 2019. Tuning, measurement and prediction of the impact of freezing on product morphology: a step toward improved design of freeze-drying cycles. Drying Technol. 37 (5), 579–599. https://doi.org/10.1080/07373937.2018.1528451.

Pisano, R., Artusio, F., Adami, M., Barresi, A.A., Fissore, D., Frare, M.C., et al., 2023. Freeze-drying of pharmaceuticals in vials nested in a rack system—part I: freezing behaviour. Pharm. 15 (2), 635. https://doi.org/10.3390/pharmaceutics15020635.

Pisano, R., Capozzi, L.C., 2017. Prediction of product morphology of lyophilized drugs in the case of vacuum induced surface freezing. Chem. Eng. Res. Des. 125 (1), 119–129. https://doi.org/10.1016/j.cherd.2017.07.004.

Pisano, R., Fissore, D., Barresi, A.A., 2011. Heat transfer in freeze-drying apparatus. Developments in Heat Transfer. InTech, Rijeka (Croatia), pp. 91–114. https://doi.org/10.5772/23799.

Pisano, R., Semeraro, J., Artusio, F., Barresi, A.A., 2024. Insights into thermal interactions in frozen pharmaceutical vials: effects on ice nucleation times and inhibition. Pharm. Res. 41 (1), 1285–1297. https://doi.org/10.1007/s11095-024-03713-2.

Searles, J.A., Carpenter, J.F., Randolph, T.W., 2001. The ice nucleation temperature determines the primary drying rate of lyophilization for samples frozen on a temperature-controlled shelf. J. Pharm. Sci. 90 (7), 860–871. https://doi.org/10.1002/jps.1039.

Singh, R.P., Medina, A.G., 1989. Food Properties and Computer-Aided Engineering of Food Processing Systems, 1st Ed. Springer, Dordrecht.

Velardi, S.A., Barresi, A.A., 2008. Development of simplified models for the freeze-drying process and investigation of the optimal operating conditions. Chem. Eng. Res. Des. 86 (1), 9–22. https://doi.org/10.1016/j.cherd.2007.10.007.